doi:10.1093/jmcb/mjr001
Published online February 8, 2011

Article

Control of embryonic stem cell metastability by L-proline catabolism

Laura Casalino†, Stefania Comes†, Giuseppina Lambazzi, Benedetta De Stefano, Stefania Filosa, Sandro De Falco, Dario De Cesare, Gabriella Minchiotti*, and Eduardo Jorge Patriarca*

Stem Cell Fate Laboratory, Institute of Genetics and Biophysics "A. Buzzati-Traverso", CNR, Naples, Italy
* Correspondence to: Eduardo Jorge Patriarca, Tel: +39-081-6132431; E-mail: patriarca@igb.cnr.it; Gabriella Minchiotti, Tel: +39-081-6132357; E-mail: minchiotti@igb.cnr.it

The molecular mechanisms controlling mouse embryonic stem cell (ESC) metastability, i.e. their capacity to fluctuate between different states of pluripotency, are not fully resolved. We developed and used a novel automation platform, the *Cell*^{maker}, to screen a library of metabolites on two ESC-based phenotypic assays (i.e. proliferation and colony phenotype) and identified two metabolically related amino acids, namely L-proline (L-Pro) and L-ornithine (L-Orn), as key regulators of ESC metastability. Both compounds, but mainly L-Pro, force ESCs toward a novel epiblast stem cell (EpiSC)-like state, in a dose- and time-dependent manner. Unlike EpiSCs, L-Pro-induced cells (PiCs) contribute to chimeric embryos and rely on leukemia inhibitor factor (LIF) to self-renew. Furthermore, PiCs revert to ESCs or differentiate randomly upon removal of either L-Pro or LIF, respectively. Remarkably, PiC generation depends on both L-Pro metabolism (uptake and oxidation) and *Fgf5* induction, and is strongly counteracted by antioxidants, mainly L-ascorbic acid (vitamin C, Vc). ESCs ↔ PiCs phenotypic transition thus represents a previously undefined dynamic equilibrium between pluripotent states, which can be unbalanced either toward an EpiSC-like or an ESC phenotype by L-Pro/L-Orn or Vc treatments, respectively. All together, our data provide evidence that ESC metastability can be regulated at a metabolic level.

Keywords: embryonic stem cells, L-proline, vitamin C, colony phenotype, pluripotent states, metastability

Introduction

Two types of pluripotent stem cells have been isolated from mouse embryos: embryonic stem cells (ESCs), derived from the blastocysts of pre-implantation embryos (Evans and Kaufman, 1981; Martin, 1981), and epiblast stem cells (EpiSCs), originating from late epiblast or primitive ectoderm (PrE) of early post-implantation embryos (Brons et al., 2007; Tesar et al., 2007). Although sharing an unlimited self-renewal capacity, ESCs and EpiSCs differ by gene expression profile, growth factors/signaling reliance, and colony morphology. Although the SON triade of transcription factors (*Sox2*, *Oct4*, and *Nanog*) (Mitsui et al., 2003; Masui et al., 2007; Niwa, 2007) is highly expressed in both cell types, ESCs display a *Rex1*$^{+}$/*Fgf5*$^{-}$ phenotype, while EpiSCs exhibit a *Rex1*$^{-}$/*Fgf5*$^{+}$ phenotype. *Rex1 (Zfp42)* encodes a transcription factor highly expressed in the inner cell mass (ICM) but down regulated in the PrE (Rogers et al., 1991; Pelton et al., 2002), whereas *Fgf5* (fibroblast growth factor 5 gene), almost absent in ICM, is highly induced in PrE (Haub and Goldfarb, 1991). In addition, ESCs depend on leukemia inhibitory factor (LIF) and bone morphogenetic protein 4 (BMP4) (Ying et al., 2003) to proliferate remaining undifferentiated, whereas EpiSCs rely on basic FGF (bFGF) and Activin/TGFβ signaling (Brons et al., 2007; Tesar et al., 2007). Furthermore, while ESCs grow developing three-dimensional rounded colonies with regular borders, EpiSCs proliferate forming bi-dimensional flat-shaped colonies with irregular borders. Recently, a near-pluripotent stem cell type, namely FGF, Activin, and BIO-derived stem cells (FAB–SCs), was isolated from the ICM of blastocysts (Chou et al., 2008). Similarly to EpiSCs, however, FAB-SCs rely on bFGF/Activin and develop flat-shaped monolayer colonies.

It has been recently reported that cultured ESCs consist of a heterogeneous cell population fluctuating between different states of pluripotency. At the extremes of this phenotypic variation cells display identifiable features of ESCs or EpiSCs, respectively (Hayashi et al., 2008; Toyooka et al., 2008; Kalmar et al., 2009). Moreover, early primitive ectoderm-like cells (EPLCs) displaying a *Rex1*$^{-}$/*Fgf5*$^{+}$, flat-shaped phenotype, and bFGF/Activin reliance were generated incubating ESCs in HepG2 (hepatocellular carcinoma) cell line-conditioned medium (Rathjen et al., 1999), and EpiSC-like cells developed culturing ESCs in a medium containing high levels of bFGF/Activin without fetal bovine serum (FBS) and LIF (Guo et al., 2009). On the other hand, a stringent ESC medium (LIF plus FBS) was sufficient to revert both EPLCs and EpiSCs to an ESC-like state (Rathjen et al., 1999; Hanna et al., 2009). Based on these data,

†These authors contributed equally.
Received September 13, 2010. Revised December 4, 2010. Accepted December 14, 2010.

it clearly emerges that: (i) the ESC → EpiSC-like phenotypic transition is reversible and regulated by growth factors; (ii) cells relying on LIF/STAT3 and BMP4 signaling grow stacked (multilayered), whereas cells depending on bFGF and Activin/TGFβ signaling proliferate as a monolayer.

Recently, considerable efforts have been focused on the development of new tools and methodologies to identify extrinsic factors/small molecules able to modulate the pluripotent state of ESCs. Here, we used an innovative robotic platform, the *Cell*^{maker}, designed to automate the screening of compound collections on ESC proliferation, colony morphology, or differentiation and identified, through the screening of a library of metabolites, key regulators of ESC proliferation and ESC → EpiSC transition.

Results

The Cell^{maker}*: a fully automated platform combining HTS with ESC-based assays*

We have designed the *Cell*^{maker} to perform high-throughput molecular screenings on ESC-based phenotypic assays (proliferation/differentiation). The robotic system (Figure 1A) was assembled integrating robot-accessible instruments (incubators, multi-signal reader) with a liquid-handling workstation through three different transfer units (a robotic arm, a linear transfer trail and a grip) (Supplemental Figure S1). The *Cell*^{maker} is guided by a software allowing a dynamic scheduling of operations ranging from a single task, such as 'cell plating', to multi-task processes as 'colony phenotype' assay. Furthermore, lab-set up protocols improved the *Cell*^{maker} performance by providing a quantifiable readout for each phenotype analyzed. In its current configuration, the *Cell*^{maker} can handle, in complete automation, up to 4000 mini-cultures (96-well format) of ESCs. Notably, we established that the *Cell*^{maker} executes both ESC proliferation and colony formation assays with high standards of reliability and accuracy (Supplemental Figure S2; data not shown). These results prompted us to exploit the *Cell*^{maker} technology to search for metabolites acting as ESC regulators.

L-Pro and L-Orn induce ESC proliferation

We used the *Cell*^{maker} to screen a homemade assembled library of metabolites on the proliferation of TBV2-derived cells expressing enhanced green fluorescence protein (EGFP) under the control of the housekeeping β-actin gene promoter (β-actin/EGFP cells), and identified L-Pro and L-Orn as putative inducers of ESC proliferation (Figure 1B). Indeed, mini-cultures of cells supplemented with L-Pro or L-Orn emitted fluorescent signals 2-fold higher than untreated ones (Figure 1B). Most remarkably, cells cultured in the presence of L-Pro or L-Orn developed wider colonies compared with untreated controls (Figure 1C). Moreover, both amino acids stimulated ESC proliferation in a dose-dependent manner, although with different kinetics (Figure 1D): at concentrations ranging from 30 μM to 1 mM, L-Pro showed a higher efficacy than L-Orn, inducing the greatest proliferation response already at 100 μM. A 20-fold higher concentration of L-Orn (i.e. 2 mM) was required to achieve a similar pro-proliferative effect. We then used the parental (i.e. non-engineered) TBV2 cells and, in agreement with the *Cell*^{maker} results, the cell density of cultures treated with L-Pro was ∼2-fold higher compared with untreated ESCs (Figure 1E).

To assess the cell line-specificity of L-Pro effect, we used different unrelated cells. Remarkably, all the ESC lines assayed were susceptible, at a different extent, to L-Pro addition (Figure 1F); conversely, none of the non-ESC lines assayed responded to L-Pro stimulation (Figure 1F), suggesting that L-Pro responsiveness is a specific feature of ESCs.

L-Pro and L-Orn force ESCs toward an EpiSC-like phenotype

Given the pro-proliferative effect of L-Pro and L-Orn, we asked whether these metabolites might also affect the morphology of ESCs. To this end, we further exploited the *Cell*^{maker} to assay our library of metabolites on the colony phenotype of wild-type TBV2 cells (Figure 2). Unexpectedly, the colonies assumed a clear-cut EpiSC-like morphology upon treatment with either L-Pro or L-Orn (Figure 2A). These results were further validated by means of manual assays (Figure 2B). As expected, ∼90% of the colonies in untreated controls displayed a characteristic round-shaped three-dimensional (domed) morphology, with uniform and birefringent edges. Conversely, ∼90% of the colonies developed in the presence of L-Pro showed a flat-shaped two-dimensional phenotype with irregular edges (Figure 2B). Remarkably, densely packed cells of 'typical' domed colonies and epithelial-like cells of 'atypical' flat colonies displayed a similar ultrastructure with a high nuclear–cytoplasmic ratio, a characteristic trait of pluripotent stem cells, prominent nucleoli and rod-shaped mitochondria (Figure 2C). Unlike L-Pro, treatment with L-Orn, even at high concentrations, resulted in only ∼50% of the cell colonies displaying a flat-shaped morphology, indicating that L-Orn induces the phenotypic transition less efficiently than L-Pro (Figure 2B). Noteworthy, no difference was observed in the colony-formation efficiency of TBV2 ESCs plated either in the presence or in the absence of L-Pro/L-Orn (≥96%; see "Materials and methods"). Remarkably, even at high L-Pro concentrations, a significant fraction (up to ∼10%) of the colonies persistently displayed the typical ESC shape, indicating that a subpopulation of ESCs are unresponsive to L-Pro.

L-Pro and L-Orn induce the phenotypic switch in a dose- and time-dependent manner

Physiological concentrations of L-Pro in human and mouse plasma range from 0.1 mM to 0.5 mM. We thus used the *Cell*^{maker} to evaluate the effect of increasing concentrations of both L-Pro and L-Orn on the colony phenotype of TBV2 ESCs. This analysis revealed significant differences in the efficiency of both amino acids to induce the ESC → EpiSC-like transition (Figure 2D). Indeed, low amounts of L-Pro (∼30 μM) already induced the formation of a significant fraction (∼25%) of atypical (flat or mixed shape) cell colonies compared with control (4%–8%). Differently, a 30-fold higher concentration of L-Orn (i.e. 1 mM) was required to stimulate a similar phenotypic variation (Figure 2D). The results were then validated in manual assays and, remarkably, up from 75 μM L-Pro, the majority of the colonies (85%–90%) displayed a clear-cut EpiSC-like morphology, after 4 days in culture (Figure 2E). Thus, physiological concentrations of L-Pro were sufficient to trigger the phenotypic switch of ESCs. Moreover, the

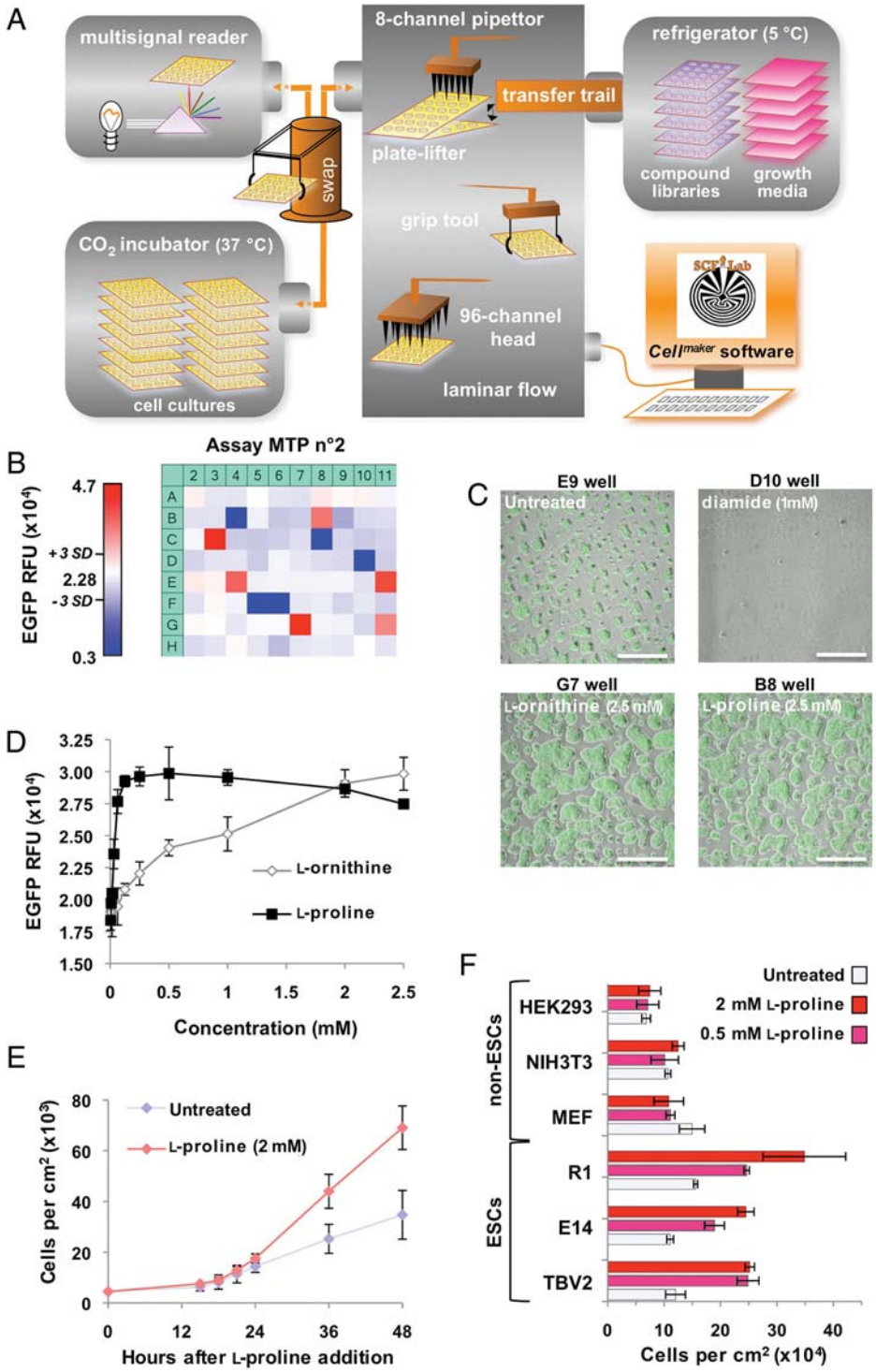

Figure 1 Identification of L-Pro and L-Orn as inducers of ESC proliferation. (**A**) Schematic illustration of the *Cell*^{maker} configuration. (**B**) Automated screening on proliferation of EGFP-marked ESCs. Relative fluorescence units (RFU) collected (36 h after metabolites addition) from microtiterplate (MTP) no. 2 are visualized following a colorimetric scale (plate mean = 2.28×10^4 RFU). (**C**) Photomicrographs (fluorescence/phase contrast overlay) of EGFP-marked ESCs grew at the indicated positions of MTP no. 2. Scale bar, 75 μm. (**D**) Dose-response curve of L-Pro/L-Orn on ESC proliferation (automated assay). Fluorescence data, measured 36 h after metabolites addition, are shown. (**E**) Manual proliferation assay. Wild-type TBV2 ESCs were grown in gelatin-coated feeder-free 6-well plates and counted at the indicated times. (**F**) Cell-type specific effect of L-Pro. Cells were grown for 36 h with or without L-Pro. TBV2, R1, E14 are ESCs; mouse embryonic primary fibroblasts (MEF, passage 8), mouse embryonic fibroblast cell line (NIH3T3) and human embryonic kidney (HEK293) cell lines are non-ESCs. (**D–F**) Data are means ± SD ($n = 3$).

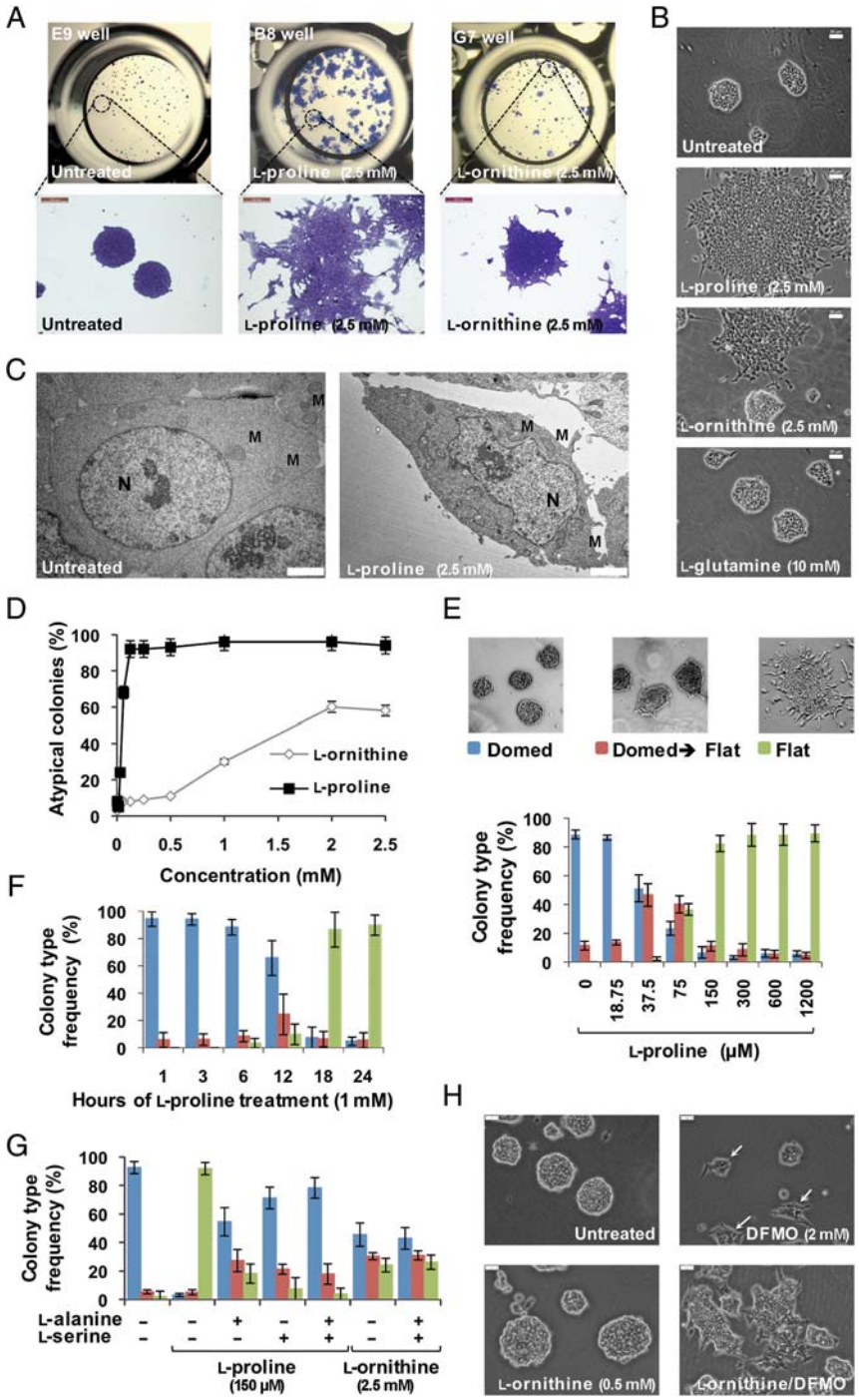

Figure 2 L-Pro and L-Orn induce a morphological transition of ESCs. (**A**) Automated screening on 4-day CPA of wild-type TBV2 ESCs. Bright field photomicrographs of crystal violet-stained cell colonies: E9 well (untreated), B8 well (L-Pro), and G7 well (L-Orn) are shown. Enlargements of the boxed regions are also shown. Scale bar, 50 μm. (**B**) Manual 4-day CPA. Phase contrast photomicrographs showed colony morphology of untreated or L-Pro, L-Orn, L-Gln-treated cells. Scale bar, 50 μm. (**C**) TEM photomicrographs of ESCs untreated or treated with L-Pro. N, nucleus; M, mitochondrion. Scale bar, 200 nm. (**D**) Dose-response effect of L-Pro/L-Orn, automated 4-day CPA. The mean percentage of atypical colonies (flat and intermediate phenotype) counted at each L-Pro concentration is shown. (**E**) Dose-dependent effect of L-Pro on cell morphology of a 4-day CPA. Upper panels show morphology-based cell colony classification: round-shaped (blue), mixed domed → flat (red) and flat-shaped (green). The percentage of colony types measured at each L-Pro concentration is shown (lower panel). (**D** and **E**) Data are means ± SD ($n = 5$). (**F**) Time-dependent L-Pro effect on colony morphology (4-day CPA). L-Pro was removed from the culture, by medium replacement, at the indicated time points. The percentage of colony types (**E**) is shown. (**G**) Effect of L-alanine/L-serine on L-Pro and L-Orn activity. ESCs were seeded in the presence of L-Pro (150 μM) or L-Orn (2.5 mM) with or without L-Ala and/or L-Ser (2.5 mM). The percentage of each colony type after 4 days in each culture condition is shown. Data are means ± SD ($n = 3$). (**H**) Effect of DFMO on L-Orn activity. ESCs were plated with L-Orn (500 μM) with or without DFMO (2 mM). Phase contrast photomicrographs of the cell colonies at day 4 are shown. Scale bar, 50 μm.

L-Pro-induced phenotypic transition was achieved seeding ESCs (TBV2 and E14 lines) at a clonal density (from 10 to 50 cells/cm^2) on gelatin-coated feeder-free plates (Supplemental Figure S3A and D). It is worth nothing that, the phenotypic transition was strongly influenced by the density of feeder cells (Supplemental Figure S3B). Indeed, a high-density layer of mouse embryo fibroblasts (MEFs), but not their conditioned medium, forced ESCs to developed round-shaped colonies even at high L-Pro concentrations; whereas, on a low-density layer of MEFs, ESCs developed flat-shaped (monolayer) colonies. Interestingly, we noticed that fibroblasts represented a physical barrier for the spreading of colonies (Supplemental Figure S3B), confirming that, unlike ESCs, L-Pro-induced cells (PiCs) are unable to grow forming multilayered colonies. Worth noting, round-shaped colonies developed in the presence of L-Pro on a high-density layer of MEFs retain pluripotency markers, such as alkaline phosphatase activity (Supplemental Figure S3C).

In order to determine the time required for L-Pro to induce the EpiSC-like morphology, we performed a L-Pro time course on a colony assay by progressively withdrawing L-Pro from the culture medium (Figure 2F). Eighteen hours of L-Pro treatment were sufficient to trigger efficiently the morphological transition (~90% of flat-shaped colonies) and, thus, the commitment of ESCs toward an EpiSC-like phenotype.

The induction of the EpiSC-like phenotype relies on intracellular L-Pro

L-serine (L-Ser) and L-alanine (L-Ala) compete with L-Pro for different neutral amino acid uptake/transport systems, such as ATA2 (also named SNAT2 or SAT2), in many cell lines (Figure 3A). Interestingly, neither L-Ser nor L-Ala was recognized as a hit in our screening. To first confirm the inability of these amino acids to influence ESC colony phenotype, we performed a manual colony assay using L-Pro in the presence of 15-fold excess of L-Ser and L-Ala, provided either alone or in combination (Figure 2G). Remarkably, the simultaneous addition of both competitors to the culture medium inhibited, almost completely, L-Pro but not L-Orn activity (Figure 2G), thus suggesting that L-Pro internalization was required to induce the phenotypic transition. Worth noting, several ESC lines are cultured in medium supplemented with a mixture of non-essential amino acids (NEAA) containing, among others, L-Pro, L-Ser and L-Ala (100 μM each). We thus performed colony assays in the presence of NEAA, seeding TBV2 cells at a clonal density (25 cells/cm^2), and found that ~50% of the colonies displayed a flat morphology (data not shown). Interestingly, this fraction was significantly higher compared with the absence of NEAA (i.e. 8%–10%), but much lower compared with L-Pro treatment (85%–90%, 100 μM L-Pro). Thus, we concluded that the presence of NEAA in the culture medium may influence ESC colony phenotype.

L-Orn could either be catabolized to polyamines or converted to Δ^1-pyrroline-5-carboxylate (P5C) and, eventually, to L-Pro (Figure 3A). It is thus tempting to reason that L-Orn → L-Pro conversion might account for the L-Orn activity. Therefore, in an attempt to increase the intracellular levels of P5C or L-Pro from L-Orn, we treated the cells with α-difluoromethylornithine (DFMO), a potent suicide inhibitor of the first enzyme of

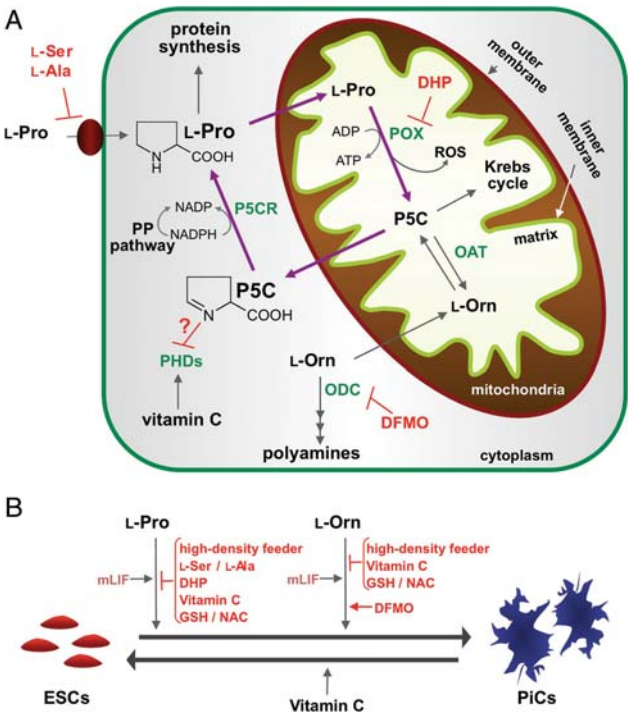

Figure 3 L-Pro and L-Orn metabolism and functions. (**A**) L-Pro and L-Orn metabolic interplay. L-Pro, L-alanine (L-Ala) and L-serine (L-Ser) share some uptake systems. Proline oxidase (POX) catalyzes L-Pro dehydrogenation to Δ^1-pyrroline-5-carboxylate (P5C) and generates reactive oxygen species (ROS). POX and P5C reductase, which converts P5C back to L-Pro in the cytoplasm, generating the proline cycle (purple arrows), a cytosol → mitochondria redox shuttle, transferring reducing equivalents generated by the pentose phosphate (PP) pathway into mitochondria for ATP production. P5C is a key intermediate bridging L-Pro to L-Orn metabolism and the Krebs cycle. OAT, ornithine-δ-aminotransferase; PDHs, prolyl hydroxylases; ODC, ornithine decarboxylase; DFMO, α-difluoromethylornithine. (**B**) Molecules and culture conditions affecting the reversible ESC ↔ PiC transition. L-Pro and L-Orn induce, in the presence of LIF, the conversion of ESCs to PiCs. This activity is counteracted by: high-density feeder cells, competitors of L-Pro uptake (L-Ser/L-Ala), antioxidants, i.e. Vc, glutathione (GSH) and N-acetyl-L-cysteine (NAC). L-Pro but not L-Orn activity is neutralized by DHP (3,4-dehydro-L-proline), a POX inhibitor. Vc treatment disturbs the ESC ↔ PiC equilibrium forcing the cells toward the ESC phenotype.

polyamines biosynthesis, i.e. ornithine decarboxylase (ODC). Interestingly, ESCs mainly developed typical round-shaped colonies when treated with a sub-optimal concentration of L-Orn (0.5 mM) (Figure 2H), whereas, they primarily gave rise to atypical flat-shaped colonies, if simultaneously treated with a sub-lethal concentration (2 mM) of DFMO (Figure 2H). Interestingly, DFMO *per se* forced ESCs toward a flat-shaped phenotype (Figure 2H), although cell proliferation was severely impaired, thus excluding a role of polyamines in the induction of the morphological transition. Conversely, our data suggest that L-Pro itself or P5C, the metabolic intermediate in L-Orn → L-Pro conversion (Figure 3A), may be the triggering factor for the EpiSC-like phenotype induction. Thus, EpiSC-like (flat-shaped) cells generated by both amino acids, L-Pro and L-Orn, were named PiCs.

POX activity is required for L-Pro- but not L-Orn-induced PiC phenotype

Once transported within cells, L-Pro can be either anabolized (protein synthesis) or eventually catabolized, i.e. oxidized for energy production (Figure 3A). Proline oxidase (POX), a mitochondrial inner membrane enzyme, catalyzes the first rate-limiting step of L-Pro degradation, i.e. its conversion to P5C (Figure 3A). Hence, we evaluated the effect of a competitive inhibitor of POX, the 3,4-dehydro-L-proline (DHP) on L-Pro (in 50 μM) activity in colony phenotype assay (CPA) at day 5 (Figure 4A and B). Interestingly, a 3-fold excess of DHP (150 μM) inhibited PiC formation almost completely (Figure 4A). Conversely, DHP was unable to counteract the L-Orn ability to induce PiCs (Figure 4A). Since L-Pro → P5C conversion is POX-dependent, while L-Orn → P5C conversion is POX-independent (Figure 3A), our data point to a key role of P5C in the molecular mechanisms underlying ESC morphological transition.

The POX inhibitor was also able to reduce the pro-proliferative effect of both L-Pro (Figure 4B) and L-Orn (data not shown), suggesting that the L-Pro cycle (Figure 3A) is involved in the induction of ESC proliferation. Indeed, L-Pro cycle activation could enhance the recovery of ATP/energy from the NADPH, mainly

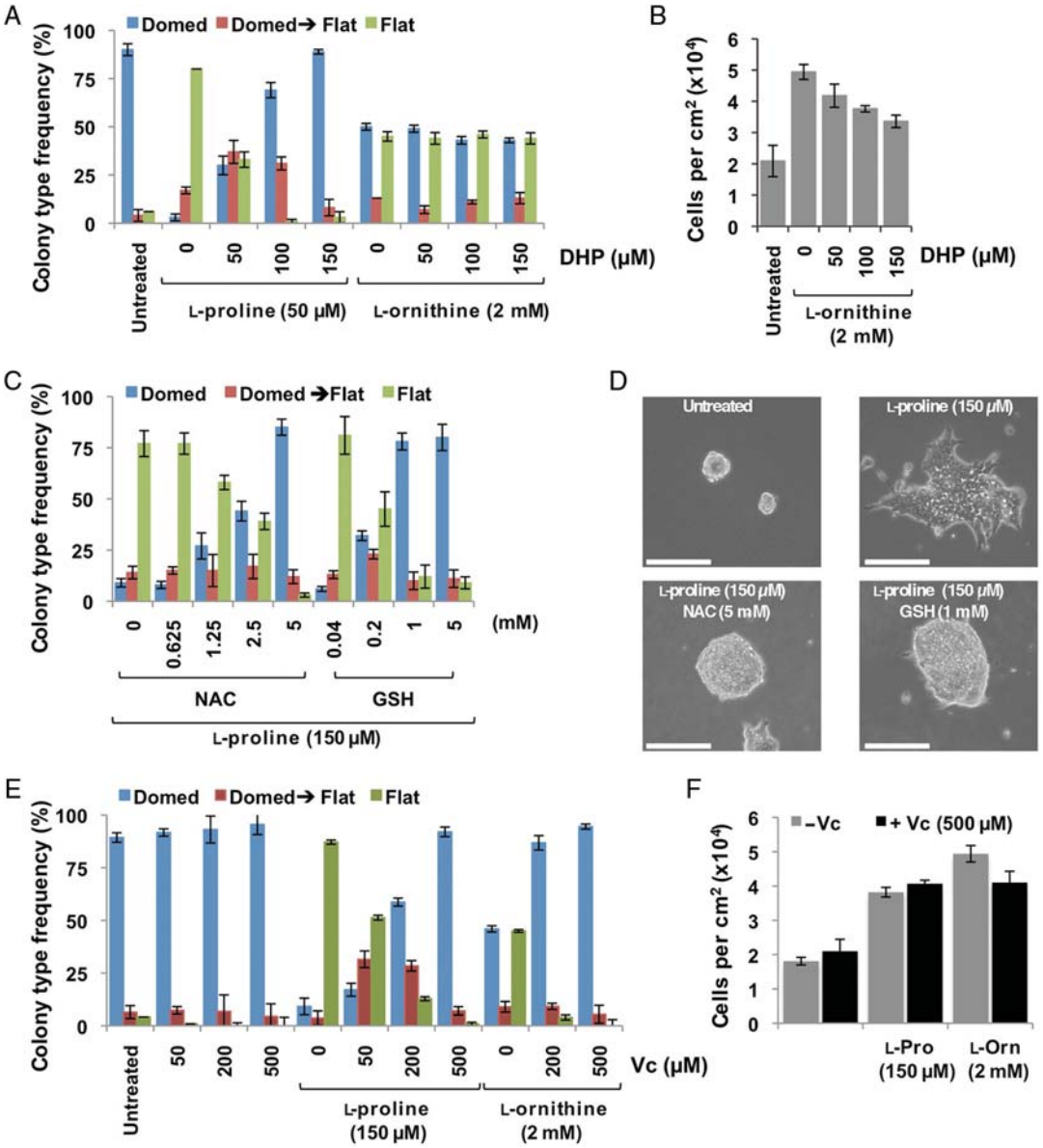

Figure 4 L-Pro requires POX activity to induce both ESC proliferation and morphological transition. (**A**) 5-day CPA: the POX inhibitor 3,4-dehydro-L-proline (DHP) affects L-Pro- but not L-Orn-induced morphological transition. (**B**) DHP inhibits L-Orn-induced proliferation. ESCs were pre-treated with DHP before addition of L-Pro (50 μM) or L-Orn (2 mM). (**C**–**E**) 5-day CPA on ESCs: L-Pro was used at the indicated concentration. (**C**) Thiol antioxidants, i.e. N-acetyl-L-cysteine (NAC) and glutathione (GSH), counteract L-Pro-induced phenotypic transition. (**D**) Phase contrast photomicrographs of representative cell colonies. Scale bar, 75 μm. (**E**) Vc counteracts L-Pro and L-Orn-induced morphological transition. (**F**) Manual proliferation assay (48 h) showing that Vc does not affect the pro-proliferative activity of L-Pro or L-Orn on ESCs. (**A**–**F**) Data are means ± SD ($n = 3$).

generated by glucose catabolism through the pentose phosphate (PP) pathway (Figure 3A). On the basis of this consideration, we assayed the effect of L-Pro and L-Orn on the proliferation/phenotype of a TBV2-derived ESC line lacking the first enzyme of the PP pathway, i.e. glucose-6-phosphate dehydrogenase (G6PD) (Paglialunga et al., 2004). Interestingly, G6PD null ESCs responded inefficiently to the pro-proliferative stimulus of both L-Pro and L-Orn and developed much smaller atypical (flat or mixed shape) colonies than the parental TBV2 cells (data not shown), thus suggesting that ESC proliferation, but not ESC → PiC transition, depends, at least to some extent, on PP pathway.

Antioxidants, mainly Vc, inhibit L-Pro- and L-Orn-mediated induction of PiCs

Reactive oxygen species (ROS) are by-products of POX activity (Figure 3A) and might thus be involved in the L-Pro-induced phenotypic transition. To get some insights into this issue, we performed ESC colony assays in the presence of increasing amount of well-known ROS scavengers (antioxidants), namely glutathione (GSH), N-acetyl-L-cysteine (NAC), and L-ascorbic acid (vitamin C, Vc). Both GSH and NAC prevented the formation of PiCs in a dose-dependent manner reaching a full counteracting activity at concentrations 7- and 30-fold higher than L-Pro (150 μM), respectively (Figure 4C and D). Conversely, Vc affected L-Pro activity already at 50 μM (i.e. 3-fold lower than L-Pro), while at 200 μM it almost completely inhibited PiC formation (Figure 4E). Moreover, Vc also blocked the L-Orn-induced transition (Figure 4E). Most remarkably, the fraction (∼10%) of atypical (flat-shaped) colonies, consistently developed by TBV2 cells in feeder-free conditions, disappeared in the presence of Vc (Figure 4E). On the other hand, neither Vc nor GSH/NAC inhibited the pro-proliferative effect of L-Pro/L-Orn (Figure 4F and data not shown).

PiCs express markers of pluripotency

To evaluate whether PiCs retained pluripotency properties, we analyzed the expression of pluripotency genes/markers (Figure 5). While comparable levels of *Sox2*, *Oct3/4*, *Nodal*, and *Cripto* transcripts were detected in ESCs and PiCs, *Nanog* transcripts were reduced (∼2-fold) in PiCs (Figure 5A). Similarly, *Gbx2* (gastrulation brain homeobox 2), *Rex1* (*Zfp42,* zinc finger protein 42 homolog), and *CRTR-1* (a transcriptional repressor of the CP2 family) were also downregulated (Figure 5A). Interestingly, *Gbx2, Rex1*, and *CRTR1* are markers of mouse ICM, and are all downregulated upon PrE formation. On the contrary, *Fut4* (fucosyltransferase 4) increased ∼10-fold in PiCs compared with ESCs. Furthermore, *Fgf5*, which is upregulated both in late epiblast and EpiSCs, was induced ∼100-fold in PiCs (Figure 5A). We then assessed the expression of SSEA1 (stage-specific embryonic antigen-1), Oct3/4, and E-cadherin (Ca^{2+}-dependent adhesion molecule) by immunofluorescence analysis (Figure 5B). Remarkably, SSEA1 and Oct3/4 were detected at the plasma membrane (SSEA1) and in the nuclei (Oct3/4) of both ESCs and PiCs. On the contrary, while E-cadherin expression was detected at the membrane of ESCs, it almost completely disappeared in PiCs (Figure 5B). Interestingly, like EpiSCs, PiCs displayed low levels of alkaline phosphatase activity (Supplemental Figure S3C). To gain deeper insights into the molecular analysis, we evaluated the expression of α-N-acetylgalactosamine (GalNAc), a surface marker of ESCs (Nash et al., 2007). Fluorescence-activated cell sorter (FACS) flow cytometry analysis showed a marked reduction in GalNAc during ESC → PiC transition (Figure 5C). Hence, all together our data indicate that PiCs display a profile of 'stemness' markers similar to that of epiblast-like cells either derived from mouse embryos or spontaneously formed in standard ESC cultures.

PiCs require L-Pro and mLIF to self-renew

To assess the self-renewal ability of PiCs, we subcultured them for several continuous passages on gelatin-coated feeder-free plates in the presence of both LIF and L-Pro (Figure 5D). Notably, as described for EpiSCs (Brons et al., 2007), PiCs are highly susceptible to trypsinization and require milder proteolytic/collagenolytic enzymatic treatments, i.e. accutase, for cell dissociation. After several passages, PiCs retained both their morphology and specific gene expression profiles, i.e. equal levels of *Oct3/4* and *SSEA1*, high *Fgf5*, low *Gbx2*, and *Rex1* levels (Figure 5D and F). Remarkably, we found that PiCs could survive to >30 passages without any appreciable loss of their phenotype (data not shown). Conversely, after five passages in the absence of L-Pro, cells reverted to ESC features as shown by morphological and molecular analysis (Figure 5E and F). Worth noting, a CPA performed plating PiCs (passage 7) at a low density and in the absence of L-Pro was sufficient to induce the PiC → ESC morphological reversion (Figure 5G). Indeed, while only ∼10% of the colonies displayed an ESC-like morphology in the presence of L-Pro, a more significative fraction, up to ∼60%, was observed in the absence of L-Pro (Figure 5G). Worth noting, the colony formation efficiency of PiCs was unaffected by L-Pro treatment (data not shown). These data indicate that the phenotypic reversion is not due to selective proliferation of ESCs subpopulation persisting in PiC cultures. Concluding, PiCs and ESCs are likely in a dynamic equilibrium and L-Pro thrusts the cells to adopt an EpiSC-like phenotype.

We established that LIF was essential to achieve the phenotypic transition (PiC induction; Figure 6A and B). Indeed, randomly differentiated cells were clearly evident already at day 3 in CPAs with L-Pro but in the absence of LIF (Figure 6A). Moreover, 2 days later (i.e. at day 5 from seeding), high levels of *Gata4* (meso-endoderm) and *Brachyury* (a pan mesodermal marker) were measured, while expression of *Sox1* and *Pax6* was almost undetectable, indicating the presence of differentiated cells (Figure 6B). Moreover, random differentiation was also observed after three rounds of subculturing in the presence of L-Pro but in the absence of LIF (Figure 6B), thus indicating that LIF was essential for PiCs to self-renew. Interestingly, it has been previously shown that EpiSCs require bFGF and Activin A to self-renew (Brons et al., 2007; Tesar et al., 2007); thus, to evaluate whether bFGF and Activin A could replace LIF requirement to support PiC self-renewal, we performed a molecular analysis after three rounds of PiC subculturing in the presence of bFGF (10 ng/ml) and Activin A (50 ng/ml), without LIF. Interestingly, while the pluripotency markers *Oct3/4* and *Nanog* were downregulated, the expression of *Gata4* and *Brachyury* (*T*) strongly

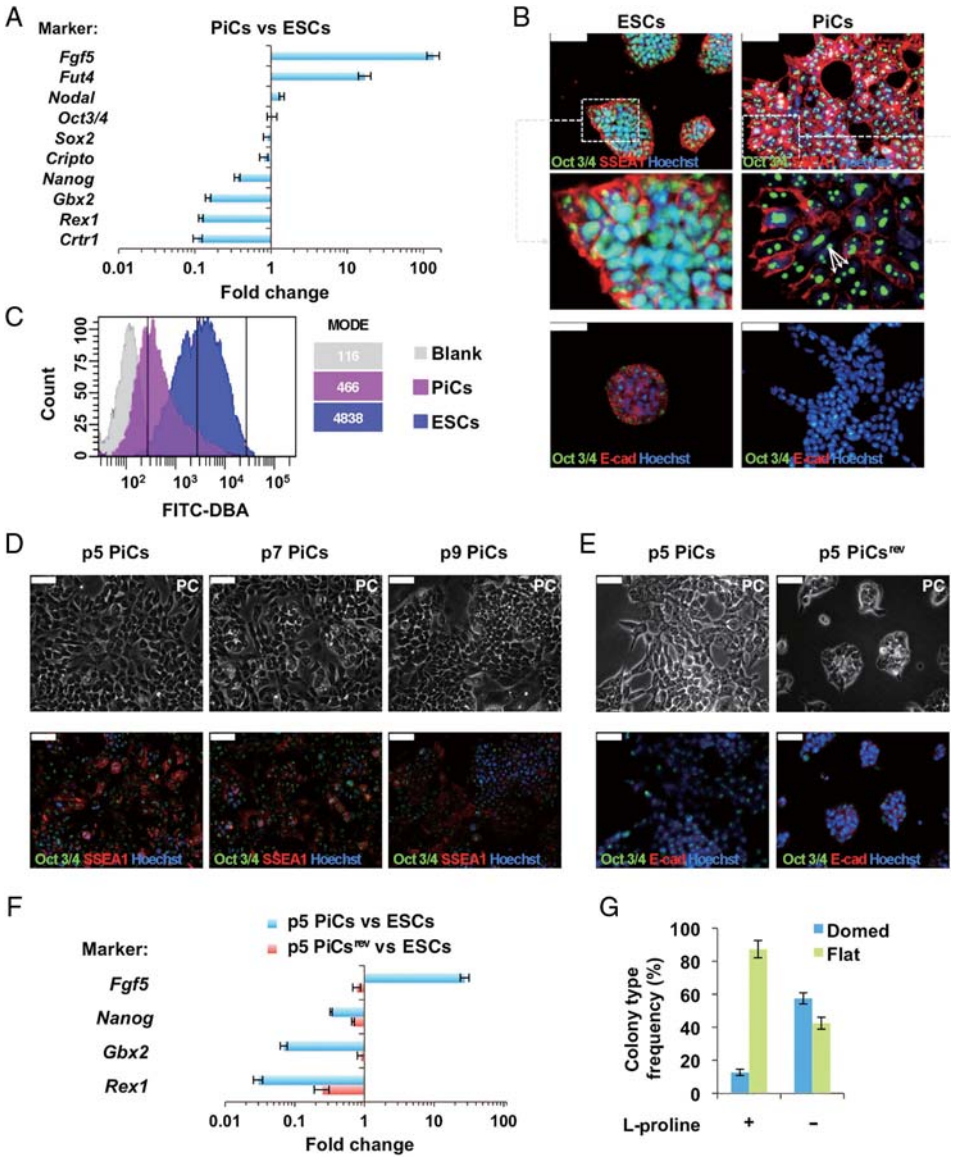

Figure 5 Molecular characterization, self-renewal properties and reversibility of PiCs. (**A**) Q-PCR analysis of selected markers in PiCs and ESCs. mRNA was normalized to GAPDH. Data are means ± SD ($n = 3$) and expressed as fold changes in gene expression of PiCs versus ESCs. (**B**) Immunostaining of ESCs and PiCs for Oct3/4, SSEA1, and E-cadherin. Nuclei were stained with Hoechst. Upper photomicrographs show Oct3/4-SSEA1 double staining of ESCs/PiCs. White arrows indicate the nucleolar localization of Oct3/4. Scale bar, 75 μm. Lower photomicrographs show Oct3/4, E-cadherin (E-cad) double staining of ESCs/PiCs. Scale bar, 50 μm. (**C**) FACS analysis of α-N-acetylgalactosamine (GalNAc) surface marker on unstained ESCs (blank, FITC-negative), FITC-DBA-stained ESCs (highly positive) and PiCs (weakly positive). (**D**) Propagation properties of PiCs. Phase-contrast and Oct3/4-SSEA1 double immunostaining photomicrographs of PiCs at subculture passage 5, 7, and 9, in the presence of L-Pro. Scale bar, 50 μm. (**E**) Effect of L-Pro withdrawal on PiC propagation. Phase-contrast and Oct3/4-E-cadherin immunostaining of cell colonies after five subculture passages (at high cell density, 2.5–3.5 × 10^4 cells/cm^2) either in the presence (p5 PiCs) or in the absence (p5 $PiCs^{rev}$) of L-Pro. Scale bar, 50 μm. (**F**) Q-PCR expression profile of specific markers in p5 PiCs and p5 $PiCs^{rev}$. mRNA was normalized to GAPDH. Data are means ± SD ($n = 3$) and expressed as fold change in gene expression of PiCs versus ESCs. (**G**) Reversion of PiCs growing at low density (5-day CPA). PiCs were plated at 1000 cells/cm^2 with or without L-Pro. Phenotypic reversion to ESCs was observed already after one subculture passage at low density, as indicated by colony type frequency distribution. Data are means ± SD ($n = 3$).

increased (Figure 6C), indicating that bFGF and Activin A, induced differentiation rather than supporting PiC self-renewal, thus being unable to replace LIF function (Figure 6C). These data indicate that LIF is required for both generation and maintenance of PiCs; furthermore, while LIF removal promotes differentiation during PiC propagation, L-Pro removal induces the reversion of PiCs toward an ESC phenotype.

PiC formation depends on Fgf5 induction

Fgf5 is a late epiblast marker during embryo development and is strongly induced in PiCs (Figure 5A). Thus, to assess if *Fgf5* exerted a functional role in establishing the PiC phenotype, silencing experiments were performed using short-hairpin RNA (shRNA), which targeted *Fgf5* mRNA sequence. Two independent ESC clones were isolated (583 and 586), with a silencing efficacy

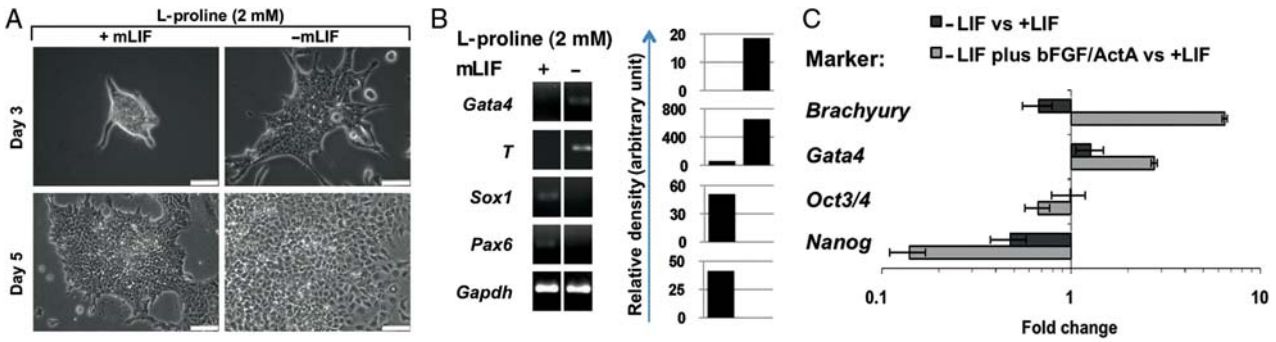

Figure 6 PiCs strictly depend on LIF to remain undifferentiated. (**A**) Phase contrast microphotographs showing cell colony morphology at days 3 and 5 in a colony phenotype assay; L-Pro was added at 2.5 mM with or without mLIF. Scale bars, 50 μm (Upper), 100 μm (Lower). (**B**) RT-PCR analysis of early-differentiation markers: *Gata4* (mesoendodermal), *T* (Brachyury, mesodermal), *Sox1* and *Pax6* (neuroectodermal). *Gapdh* was used as an internal control. Right-side histograms refer the densitometric analysis of amplification results, normalized to *Gapdh*. (**C**) PiCs were subcultured for three passages either with LIF or without LIF +/− bFGF/Activin A. Q-PCR analysis of pluripotency markers (*Nanog* and *Oct3/4*) and mesodermal markers (*Brachyury* and *Gata4*) reported as fold changes in gene expression of PiCs −LIF or PiCs −LIF +bFGF/Activin A versus PiCs +LIF (control). mRNA was normalized to *Gapdh*, data are means ± SD ($n = 3$).

of ∼40% and 85% in the presence of L-Pro, respectively (Figure 7C); these clones were used in CPAs in the presence of L-Pro (50 μM–1 mM). *Fgf5*-silenced ESCs were less responsive to L-Pro compared with control (non-targeting control vector); indeed, the fraction of cells unresponsive to L-Pro stimulus (i.e. maintaining the typical domed ESC phenotype) increased as the level of *Fgf5* transcripts decreased (Figure 7A and B). In line with these results, the expression of ESC-specific markers, such as *Rex1* and *Gbx2*, increased (Figure 7C). Moreover, in the presence of L-Pro, *Fgf5*-silenced ESCs developed smaller flat-shaped colonies compared with control (Figure 7B). Remarkably, the L-Pro-unresponsive phenotype was completely reverted, in a dose-dependent manner, upon addition of recombinant FGF5 protein to *Fgf5*-silenced ESCs (Figure 7D). All together these data pointed to a functional role of *Fgf5* expression in the L-Pro-induced ESC → PiC-like transition.

PiCs are pluripotent stem cells that retain differentiation potential both in vitro and in vivo

We explored the differentiation potential of PiCs both *in vitro* and *in vivo*. We first used the embryoid body (EB)-based cardiac differentiation protocol (Maltsev et al., 1993) and showed that PIC-derived EBs were able to generate areas of contracting cardiomyocytes (beating foci, data not shown). Cardiac differentiation was confirmed by immunofluorescence, using α-myosin heavy chain (α-MHC) antibodies (Figure 8A), and Q-PCR for gene expression analysis of cardiac mesoderm specific markers such as *Nkx2.5* (Figure 8C). Notably, expression of *Afp* (α-fetoprotein) was also strongly induced in PiC-derived EBs (Figure 8C), suggesting that PiCs could also differentiate into mesendoderm derivatives.

PiCs were also fully capable to differentiate into neurons and glia (Fico et al., 2008) as shown by immunofluorescence using anti β-III tubulin and GFAP (glial fibrillary acidic protein) antibodies, which mark neurons and glia, respectively (Figure 8B), and Q-PCR analysis of neural specific markers *Pax6* (neuroectoderm) and *Nfm* (neurons) (Figure 8C).

Moreover, we evaluated whether PiCs could give rise to teratomas *in vivo*. Upon injection into immunocompromised mice, PiCs generated teratomas characterized by the presence of different tissues, such as connective, cartilage, muscle, and epithelial tissues (Figure 8D), providing evidence of their pluripotency properties *in vivo*.

Finally, to further explore the developmental potential of PiCs *in vivo*, we evaluated their ability to contribute to chimeric embryos. Thus, we injected EGFP-labeled PiCs into blastocysts and found that donor PiCs contributed to development of chimeric embryos (Figure 8E) with high frequency (9 out of 10 embryos). Comparable results were obtained using ESCs reverted from PiCs (PiCs^{rev}) after subculturing in the absence of L-Pro (passage 5; data not shown). Overall, these results indicate that PiCs have full capacity to differentiate into the three embryonic germ layers *in vivo*.

Discussion

Over the last few years, the identification of new regulators of stem cell proliferation and/or differentiation, which are essential to realize the potential of regenerative medicine, has been greatly facilitated by the application of automation technologies. We successfully used a novel robotic platform, the *Cell^{maker}*, on phenotype-based screenings (i.e. ESC proliferation/CPAs) and identified two metabolically related amino acids, namely L-Pro and L-Orn, as ESC regulators. Worth noting, a third metabolite was found, namely L-Lysine, which acts as a potent inhibitor of ESC proliferation (our unpublished data). Interestingly, a similar inhibitor effect of L-lysine on HeLa cell proliferation was early reported (Eagle, 1955). In line with our findings, Washington et al. (2010) very recently reported that L-Pro induces differentiation of ESCs, even if, conversely to the *Cell^{maker}* strategy, this finding was obtained through conventional multi-step, time-consuming, biochemical processes implying: chromatographic fractionation of HepG2-conditioned medium, evaluation of the biological activity of all obtained fractions, and resolution of the chemical composition of each active fraction.

The first response of ESCs to L-Pro or L-Orn is a significant induction of proliferation; later on, proliferating ESCs undergo a phenotypic transition that results in the generation of EpiSC-like

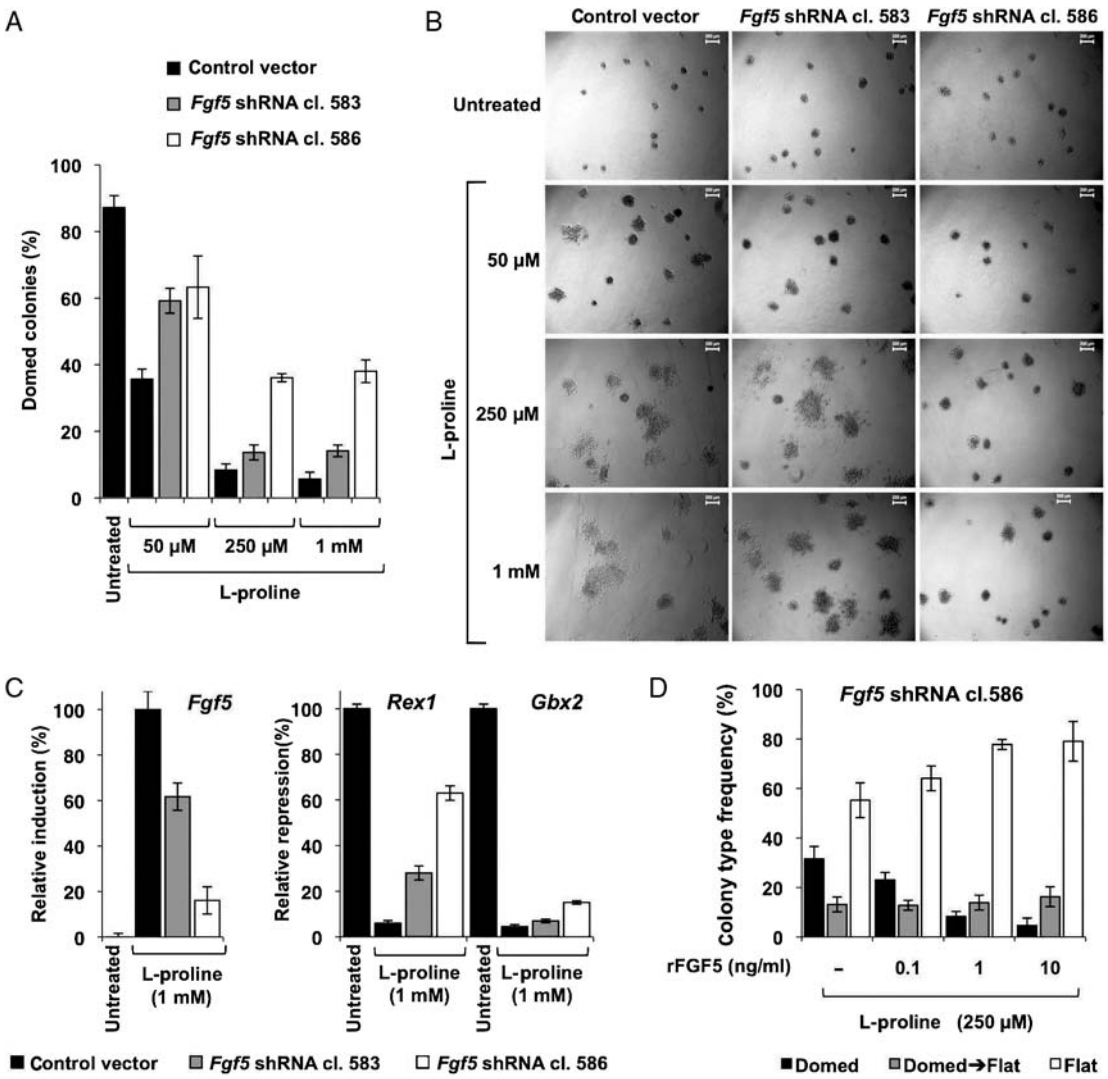

Figure 7 *Fgf5* silencing affects PiC generation. (**A** and **B**) Effect of *Fgf5* silencing on L-Pro-induced phenotypic transition: comparison between cell colonies developed by *Fgf5*-silenced (clones 583 and 586) or control (non-targeting vector) ESC clones. (**A**) The percentage of colony types is shown. Data are means ± SD ($n = 3$). (**B**) Cell colony morphology of the *Fgf5*-silenced ESC clones. Scale bars, 200 μm. (**C**) Q-PCR analysis of specific markers in *Fgf5*-silenced ESC clones. Data are expressed as percentage of *Fgf5* induction (relative to control ESCs, treated with L-Pro) and *Rex1*/*Gbx2* repression (relative to control ESCs, untreated). Data are means ± SD. (**D**) Dose-dependent effect of recombinant FGF5 protein on the colony phenotype of *Fgf5*-silenced ESCs (clone 586). Data are means ± SD ($n = 3$).

cells. Since L-Orn shows a ~20-fold lower effectiveness than L-Pro, and its activity likely depends on its conversion into L-Pro, cells generated by both these amino acids were named PiCs. PiCs are similar to pluripotent EpiSCs by different criteria, such as colony morphology, susceptibility to trypsinization, gene expression profile, and pluripotency, but differ in growth factors/signaling reliance, since they strictly depend on LIF to proliferate remaining undifferentiated, while EpiSCs rely on FGF/TGFβ signaling (Brons et al., 2007; Tesar et al., 2007). More interestingly, unlike EpiSCs, PiCs efficiently contribute to chimeric embryos. Notably, PiCs promptly revert to the ESC phenotype after removal of L-Pro, indicating that ESCs and PiCs correspond to different metastable pluripotent states.

Worth nothing, our data suggest that both generation (ESC → PiC transition) and self-renewal of PICs depend on L-Pro oxidation, catalyzed by a mitochondrial enzyme, i.e. POX. In correlation, it has been recently reported that self-renewing divisions of ESCs depend on another amino acid, i.e. threonine, and particularly on its oxidation, catalyzed by a mitochondrial enzyme, i.e. threonine dehydrogenase (Dejosez et al., 2010). Hence, our data support the intriguing idea that metabolism represent an almost unexplored level of stem cell pluripotency control (Dejosez et al., 2010). Notably, the almost undetectable level of POX activity in fibroblasts (Semon and Phang, 1991) may explain their inability to proliferate in response to L-Pro. Thus, our data suggest that L-Pro may be used to improve protocols for deriving induced pluripotent stem (iPS) cells from fibroblasts, by selectively promoting ESC/iPS rather than fibroblast proliferation.

Interestingly, the *in vitro* ESC → EpiSC-like transition induced by L-Pro is reminiscent of the *in vivo* blastocyst → epiblast transition occurring during mouse embryo implantation.

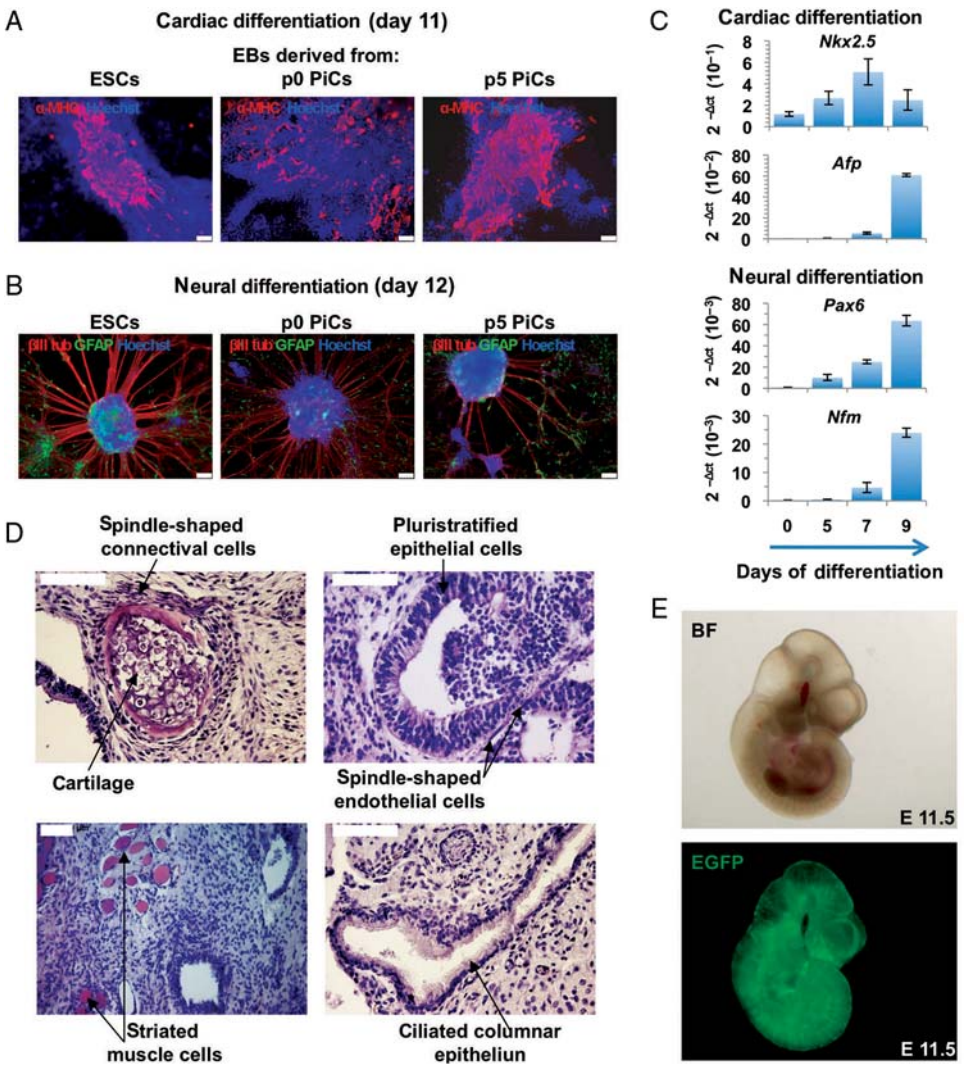

Figure 8 PiCs are pluripotent both *in vitro* and *in vivo*. (**A** and **B**) PiCs differentiate both into cardiomyocytes and neurons *in vitro*. (**A**) Cardiac differentiation. ESC- and PiC-derived embryoid bodies showing areas of α-myosin heavy chain (α-MHC) positive cells; nuclei were stained with Hoechst. Scale bar, 100 μm. (**B**) Neural differentiation. Immunostaining with anti β-III tubulin and GFAP antibodies of 12-day-old differentiated ESCs and PiCs, showing the presence of neurons and glial cells, respectively. Nuclei were stained with Hoechst. Scale bar, 100 μm. (**C**) Q-PCR analysis of lineage-specific markers of both mesoderm/cardiac (*Nkx2.5* and *Afp*, *α-fetoprotein*) and neuroectoderm/neuronal (*Pax6* and *Nfm*) differentiation of PiCs. mRNA was normalized to GAPDH. Data are means ± SD ($n = 3$). (**D**) Hematoxylin and eosin stained histological sections of PIC-derived teratomas. Scale bars, 50 μm. (**E**) Representative photomicrographs showing high contribution of PiCs in chimeric embryos. Upper panel, bright field; lower panel, EGFP expression of a chimeric embryo (11.5 d.p.c.) from donor PiCs labeled with EGFP.

Consistently, induction of *Fgf5*, a specific marker of epiblast formation, is essential for efficient ESC → PiC transition. Intriguingly, embryo implantation requires extensive degradation of the uterine extra-cellular matrix (ECM) by metalloproteases/collagenases secreted at the fetal–maternal interface (McEwan et al., 2009). Since the ECM is mostly (80%) composed of collagen, which is a L-Pro-rich protein (L-Pro and hydroxy-L-Pro together constitute over 25% of collagen amino acids), the level/availability of free L-Pro should increase during embryos implantation. Thus, it is tempting to speculate that L-Pro metabolism may have a role in the complex signaling mechanisms triggering the blastocyst → epiblast transition.

Our data point to a key role of P5C, the metabolic intermediate of L-Pro ↔ L-Orn interconversion, in the molecular mechanisms underlying morphological transition of ESCs. P5C may be converted into intermediates of Krebs cycle (Figure 3), which in turn modulate GPCR (G protein-coupled receptor)-dependent signaling (He et al., 2004). Interestingly, the morphology of the colonies developed by human ESCs and hiPS cells is under the control of GPCR signaling (Nakamura et al., 2009). In our CPAs, however, α-ketoglutarate, succinate, fumarate, and citric acid all failed to induce PiC formation (our unpublished data), suggesting that P5C exert its morphogenetic activity independently of the Krebs cycle intermediates.

Different reducing agents (GSH, NAC, Vc) are capable of fully antagonizing the morphogenetic (colony phenotype) but not the pro-proliferative activity of L-Pro and L-Orn, suggesting the involvement of different pathways for the induction of proliferation and phenotypic transition. Since GSH, NAC, and Vc are well-known ROS scavengers, ROS (by-products of L-Pro oxidation via

POX, Figure 3) could be involved in the control of ESC → PiC transition but not cell proliferation. However, POX inhibition failed to counteract L-Orn activity. Moreover, ESC treatment with two different oxidant agents, i.e. doxorubicyn (a mitochondrial superoxide producer) and hydrogen peroxide, failed to induce the ESC → PiC transition, even at doses and times sufficient to slow down ESC proliferation (our unpublished data). Finally, oxidants were also unable to enhance the weak morphogenetic activity of L-Orn (our unpublished data). All together, these findings argue against the involvement of ROS in the induction of the ESC → PiC transition and suggest that antioxidants, particularly Vc, impair L-Pro activity likely influencing other biological functions. For instance, Vc, which is maintained in its active form (i.e. reduced) by GSH, may influence, acting as a cofactor, the reactions driven by dioxygenases, including collagen prolyl hydroxylases, hypoxia-inducible factor (HIF) prolyl hydroxylases, and histone demethylases (Shi, 2007). Thus, Vc and P5C and/or L-Pro may induce opposite effects on members of the dioxygenase superfamily, which play a key role in the regulation of reversible ESC ↔ PiC transition. Most remarkably, it has been recently reported that Vc enhances the last step (pre-iPS to iPS cells) of somatic cell reprogramming (Esteban et al., 2010), which may be correlated to PiC → ESC transition.

Materials and methods

Cell culture conditions

Wild-type mouse TBV2 (129/SvP) and R1 ESCs as well as TBV2-derived cells were maintained on a feeder layer of mitomycin C-inactivated primary MEFs; feeder-independent E14 ESCs and PiCs were cultured onto gelatin-coated plates. High glucose DMEM (Gibco, Grand Island, NY, USA) supplemented with 15% ES-screened FBS (HyClone, Logan, UT, USA), 0.1 mM β-mercaptoethanol (Sigma-Aldrich, St Louis, MO, USA), 1 mM sodium pyruvate, 2 mM glutamine, 100 U/ml penicillin/streptomycin, and 1000 U/ml recombinant LIF (Euroclone, Milano, Italy) was used as a culture medium. PiCs were harvested using accutase (Sigma-Aldrich) and cultured in the presence of L-proline (300–500 μM). bFGF (Invitrogen, Carlsbad, CA, USA) and Activin A (R&D Systems, Inc., Minneapolis, MN, USA) were used at 10 ng/ml and 50 ng/ml, respectively. HEK293, NIH3T3, and MEFS were maintained in high glucose DMEM (Gibco, Grand Island, NY, USA) supplemented with 10% FBS (Euroclone), 1 mM sodium pyruvate, 2 mM glutamine, and 100 U/ml penicillin/streptomycin. For proliferation assays, non-ESCs were plated in ESC-medium with or without L-Pro at 1.5×10^4 cells/cm^2 and grown for 36 h. Living cells of triplicate sample were counted with the cell counter Cellometer AUTO T4 (Nexcelom Bioscience, Lawrence, MA, USA) at the time points indicated in the figures.

TBV2-derived cell lines

To generate EGFP-marked ESCs, a reporter vector was constructed by inserting the BamHI/SalI CMV /chicken β-actin promoter into the pEGFP1 plasmid (Clontech, Palo Alto, CA, USA). TBV2 ESCs (2×10^7) were transfected by using the Nucleofector device (Amaxa Biosystems, Lonza, Cologne) according to the manufacturer's recommendations. Following electroporation, ~20 single-cell clones were selected by G418 and one clone with high EGFP expression, undifferentiated phenotype and *in vitro* pluripotency was chosen for further experiments.

To generate stable knock-down of *Fgf5*, TBV2 ESCs were electroporated with the linearized pLKO.1 empty vector or carrying specific shRNA clones designed to target transcripts from the *Fgf5* gene: TRCN0000067583 (target sequence: 5′-CGGGAATGTG ATGAGCTGAAA-3′), TRCN0000067585 (target sequence: CTGTAA GTTCAGGGAGAGATT), TRCN0000067586 (target sequence: GAAGCCAGTGTGTTAAGTATT), and TRCN0000067587 (target sequence: GCCCTGAACAAGAGAGGGAAA) clones from TRC-Mm1.0 mouse shRNA library (Open Biosystems, Huntsville, AL, USA). After electroporation, cells were split and shRNA stable expressing cell clones were selected by G418. Clones were validated by Q-PCR and by CPAs.

Automated cell count

For the viable count, cell suspension was diluted 1:1 with 0.2% trypan blue dye and loaded into a disposable cell counting chamber-slide slotted into the imaging-based automatic cell counter Cellometer AUTO T4. Cell concentration and cell viability were automatically determined (Cellometer Auto Counter Software) on the basis of the total cell count, the dilution factor and the trypan blue dye exclusion. Optimal cell type parameters were established by modifying default setting for mouse ESCs: Cell Diameter Max and Min adjusted to 3 and 20 μm (default 8 and 30 μm). De-cluster Edge Factor (for clumpy cell) to 0.8 (default: 0.5).

Metabolite library

A collection of 65 compounds was selected to represent a custom library of commercially available compounds (Sigma-Aldrich). The Diamide growth inhibitor was included as a negative control. Test and reference compounds were dissolved in PBS or acidified aqueous solution to make stock solutions of 50 mM. For essential amino acids, stock solutions were prepared considering a 200-molar excess with respect to DMEM composition. Stock solutions were stored at −20°C until ready for use. Three master library plates were prepared by adding compounds in random intra-plate triplicates, excluding external rows and columns, filled with PBS or aqueous acidic solution. Two additional replica sets of library plates were prepared from master plates by 1–2 serial dilutions. Control plates containing PBS alone were also included. During the screen assays, a 5 μl aliquot of compounds were automatically transferred by the *Cell*^{maker} to the assay plates (1:20 dilution), giving final concentrations of compounds of 2.5 mM (library master plates), 1.25 mM (1:2 diluted library plates), and 0.625 mM (1:4 diluted library plates) or, in the case of essential amino acids, a molar excess of 10, 5, and 2.5-folds.

Metabolite screening on automated ESC-based assays

Typically, the *Cell*^{maker} was instructed to perform workflows starting with common tasks: (i) gelatin-coating; (ii) cell plating; (iii) 6-h incubation; (iv) library addition. The ESCs were manually dissociated, counted with the Cellometer AUTO T4, opportunely diluted in complete medium for undifferentiated ESCs and

provided to the *Cell*^{maker}. The 96-head pipetting device of the *Cell*^{maker} mixed the cell suspension (300 μl, 10× up-down cycles) and dispensed 100 μl per well on gelatin-coated, barcoded, 96-well microtiterplate (MTP) (Corning Costar, Lowell, MA, USA), immediately stored back into the 37°C incubator. After a 6-h incubation to allow cell adhesion, cell culture MTPs (one at time) and the associated library MTPs were removed out of the 37°C or 4°C incubator, respectively, and the library compounds were added to the cells (5 μl per well) using the 96-head pipettor. For the proliferation assays, EGFP-marked ESCs were seeded at 1.5×10^4 cells/cm^2 ($\sim 5 \times 10^3$ cells per well) and the *Cell*^{maker} workflow proceeded as follows: (v) 36 h incubation; (vi) reading task. For the end-point reading task, cell culture MTPs, after medium removal and PBS wash, were transferred to the Synergy HT (Biotek Europe, Bad Friedrichshall, Germany) multisignal reader for the fluorescence measurement. The following settings were used: optical probe in bottom position, 20 samples/well, exciting-detecting filter set at 485/20–528/30 nm. To optimize the signal to noise ratio, black/white bottom special optic MTPs (Corning Costar) were employed. A sensitivity of 80 was chosen by scaling to high well and the autofluorescence background of cell-free MTPs was subtracted. The readout was an Excel worksheet that lists all fluorescence measurements within a specific well on the original plate. A custom Excel worksheet was created to process row measurement data, excluding columns 1 and 12, by mean centering normalization and *Z*-score transformation. The list output was converted into a matrix containing the *Z*-score values defined per every well. Hits were selected using a threshold of ± 3 SD (for *Hit* selection see also "Statistical analysis"). For CPAs, wild-type TBV2 ESCs were plated at 5×10^2 cells/cm^2 and the workflow followed with: (v) 72-h incubation; (vi) medium change/compound addition; (vii) 48-h incubation (viii) PBS wash/PFA fixation/crystal violet staining (according to Franken et al., 2006). At day 5, cell colonies were manually counted and classified as typical or atypical colonies using a Leica MZ16 FA fluorescence stereomicroscope.

Manual ESC-based assays

When indicated, ESCs were pre-incubated for 1 h with the chemicals/inhibitors (all from Sigma-Aldrich) at the specified concentrations, before addition of L-Pro or L-Orn. For proliferation assays, ESCs, seeded at $1.5–3 \times 10^4$ cells/cm^2, were grown for 36–48 h. Triplicate samples were counted by trypan blue-exclusion on the Cellometer Auto T4 (Nexcelom Bioscience, Lawrence, MA, USA) at the indicated time points. For CPAs, ESCs or PiCs were seeded at 500–1000 cells/cm^2 and grown for 4–5 days, refreshing medium and metabolites/chemicals at day 2 or 3, respectively. For rescue experiments, the recombinant human FGF5 (R&D Systems, Inc.) was added at days 2 and 4. Either living or PFA-fixed cell colonies were counted and classified as domed, flat or domed → flat. To calculate the colony formation efficiency, cells were plated at 10 cells/cm^2 in 60 mm dishes; 4 days later, the colonies were counted and referred as percentage over the number of plated cells (240): 98.3% Untreated ESCs (236 ± 2), 96.7% L-Pro-treated ESCs (232 ± 3), and 97.9% L-Orn-treated ESCs (235 ± 2).

In vitro cardiac and neural differentiation

For cardiac differentiation, ESCs/PiCs were aggregated as embryoid bodies in high glucose DMEM supplemented with 15% FBS (Euroclone). EBs were prepared by 2-day hanging drop cultures (500 cells/drop) and then grown for 3 days in suspension before allowed to adhere on gelatin-coated tissue culture dishes. Typically, areas of spontaneous contractile cardiomyocytes started appearing after 3 days in culture (day 8) and could be easily identified by Phase contrast microscopy. The serum-free mono-step neural differentiation protocol was previously described (Fico et al., 2008). Briefly, cells were seeded at 1.5×10^3 cells/cm^2 in knockout D-MEM (Gibco) supplemented with 15% knockout serum replacement (Gibco), 0.1 mM β-mercaptoethanol (Sigma-Aldrich), 2 mM glutamine, and 100 U/ml penicillin/streptomycin (Euroclone) and grown for up to 12 days. At the indicated time points, cells were either fixed for immunofluorescence analysis or collected for RNA extraction.

Teratoma formation and blastocyst injection

Seven to eight weeks old Fox Chase SCID mice (Charles River, Chatillon-sur-Chalaronne, France) were used. PiCS and ESCs were detached with accutase (Sigma-Aldrich) or trypsin (Euroclone), respectively, and resuspended in PBS without Na^+ and Mg^{2+} (Euroclone) to a concentration of 1.5×10^7 cells/ml. Cells were injected subcutaneously (200 μl, 3×10^6 cells/flank) in five animals per group and tumor growth was followed by measuring tumor diameters with a caliper. All the animals injected developed the tumor. When tumors reached on average a volume of 1.5 cm^3, they were explanted, paraformaldehyde-fixed, and embedded in paraffine following standard procedures. Five micrometer-thick deparaffined tumor sections were stained with hematoxylin-eosin for the analysis. The care and husbandry of mice and xenograft tumor experimental procedures were in accordance with European Directives no. 86/609, and with Italian D.L. 116. All the experiments were approved by the Institute of Genetics and Biophysics veterinarian. For blastocyst injection, PiCs and PiCs^{rev} were generated starting from β-actin/EGFP TBV2 ESCs. Blastocysts were collected from the uterine horns of superovulated CD-1 females mated with CD-1 males. About 40–50 cells (EGFP-marked ESCs, PiCs, and PiCs^{rev}) per blastocyst were injected, followed by transfer to the uterus of pseudopregnant recipient CD-1 mice. Embryos were dissected at 11.5 days post-coitum (d.p.c.) and EGFP green fluorescence was determined using a Leica MZ16 FA fluorescence stereomicroscope.

Immunofluorescence

Immunofluorescence analysis was performed as described previously (Fico et al., 2008). Antibodies were the following: rabbit anti-Octamer 3/4 (Abcam; Cambridge, UK), 1:400, 1 h at RT; mouse anti-SSEA1 (Cell Signaling Technology; Beverly, MA, USA), 1:200 O/N 4°C; rat anti-E-cadherin (Sigma-Aldrich), 1:100, O/N 4°C; mouse anti-βIII-tubulin (Sigma-Aldrich), 1:400, 1 h at RT; rat anti-GFAP (Dako; Glostrup, Denmark), 1:300, 1 h at RT; MF20mouse anti-myosin heavy chain (Developmental Studies Hybridoma Bank; Iowa City, IA, USA), 1:50, 2 h at RT. Appropriate fluorophore-conjugated secondary antibodies were

used for visualization: Alexa Fluor 594 and 488 (1:400; Molecular Probes, Inc., Eugene, OR, USA), Cy3 (1:400; Jackson ImmunoResearch Laboratories, West Grove, PA, USA).

Light and fluorescence microscopy

Fluorescent labeling was visualized using the DMI6000B inverted fully automated microscope with DFC 420 RGB and DFC 360FX B/W digital cameras (Leica Microsystems, Wetzelar, Germany). Histology images were acquired using the Leica DM6000B fully motorized research microscope with DFC 480 RGB and DFC 350FX B/W Leica digital cameras. The Leica FW4000 and LeicaAF6000 software were used for image acquisition/elaboration (contrast/gamma adjusting) and for generation of overlay pictures.

Transmission electron microscopy

ESCs and PiCs were fixed in 2% glutaraldehyde/4% paraformaldehyde, post-fixed in osmium tetra oxide, dehydrated, and embedded in Epon 812 (Polyscience, Niles, IL, USA). Ultra-thin (60 nm) sections were cut on a Leica ultracut UCT ultramicrotome (Leica Microsystems) and contrasted with uranyl acetate and lead citrate. Grids were examined using a Jeol JEM-1011 (Jeol, Tokyo, Japan) transmission electron microscope (TEM) (100 kV, high contrast and brightness with optimum resolution) and micrographs were taken with iTEM software (Olympus Soft Imaging System GmbH, Munster, Germany).

RT–PCR and Q-PCR

Total RNA was extracted with the Perfect Pure RNA Cultured Cell Kit (5 Prime, Inc., Gaithersburg, MD, USA), following manufacturer's instructions. Q-PCR was performed using SYBR Green PCR (Euroclone), according to manufacturer's instructions. Primers for *Sox2*, *Nanog*, *Cripto*, and *Nodal* were from Qiagen (Hilden, Germany) or described in Supplemental Table S1.

DBA staining and FACS analysis

ESCs or PiCs were trypsin-detached, PBS-washed and resuspended at 1×10^7 cells/ml in 0.1% BSA/PBS. Equal volume (100 μl) of single-cell suspension were mixed with 100 μg/ml FITC-labeled DBA (Vector Laboratories Burlingame, CA, USA) in 0.1% BSA/PBS and incubated for 30 min at 4°C with agitation. After washing, cells were resuspended in 5% FBS in PBS (500 μl) and analyzed using a FACSAria cell sorter (Becton, Dickinson and Company, Franklin Lakes, NJ, USA).

Statistical analysis

Row fluorescence data from the *Cell*^{maker} were analyzed and processed using a custom Excel Worksheet or the HTS Corrector software (Makarenkov et al., 2006) for: (i) by plate normalization (mean centering procedure); (ii) elimination of outliers (=values that deviated for >3 SD from the plate mean); (iii) topological analysis of the experimental background; (iv) *hit* selection (threshold of $\pm$3 SD). Data from manual assays were presented as the mean $\pm$ SD of triplicate samples of at least two independent experiments. Statistical comparisons were performed by variance analysis (one-way ANOVA).

Supplementary material

Supplementary material is available at *Journal of Molecular Cell Biology* online.

Acknowledgements

We are grateful to Giuseppe Martini (Department of Life Science, CNR, Rome, Italy) and the CNR Life Science Department for continuous support and to Giancarlo Troncone (University of Naples 'Federico II', Naples, Italy), our colleagues Maurizio Iaccarino, Antonio Baldini, and members of the Stem Cell Fate Laboratory for helpful discussion. We thank our colleagues Rosarita Tatè and Michele Cermola of the IGB-CNR Integrated Microscopy Facility for helping with the electron microscopy analysis. Our colleagues Vincenzo Mercadante, Valeria Tarallo and the Mouse Facility of IGB-CNR are acknowledged for technical support.

Funding

This work was supported by Associazione Italiana Ricerca sul Cancro [IG-6128 to G.M. and IG-4840 to S.D.F.]; Telethon [GGP-08120 to G.M.]; Regione Campania-Programma Operativo Regionale [CRdC WP11 to S.F., S.D.F, D.D.C., G.M. and E.J.P.]; Ministero Istruzione Università Ricerca [Medical Research in Italy RBNE08HM7T_003 to E.J.P.].

Conflict of interest: none declared.

References

Brons, I.G., Smithers, L.E., Trotter, M.W., et al. (2007). Derivation of pluripotent epiblast stem cells from mammalian embryos. Nature *448*, 191–195.

Chou, Y.F., Chen, H.H., Eijpe, M., et al. (2008). The growth factor environment defines distinct pluripotent ground states in novel blastocyst-derived stem cells. Cell *135*, 449–461.

Dejosez, M., Levine, S.S., Frampton, G.M., et al. (2010). Ronin/Hcf-1 binds to a hyperconserved enhancer element and regulates genes involved in the growth of embryonic stem cells. Genes Dev. *24*, 1479–1484.

Eagle, H. (1955). The specific amino acid requirements of a human carcinoma cell (stain HeLa) in tissue culture. J. Exp. Med. *102*, 37–48.

Esteban, M.A., Wang, T., Qin, B., et al. (2010). Vitamin C enhances the generation of mouse and human induced pluripotent stem cells. Cell Stem Cell *6*, 71–79.

Evans, M.J., and Kaufman, M.H. (1981). Establishment in culture of pluripotential cells from mouse embryos. Nature *292*, 154–156.

Fico, A., Manganelli, G., Simeone, M., et al. (2008). High-throughput screening-compatible single-step protocol to differentiate embryonic stem cells in neurons. Stem Cells Dev. *17*, 573–584.

Franken, N.A., Rodermond, H.M., Stap, J., et al. (2006). Clonogenic assay of cells *in vitro*. Nat. Protoc. *1*, 2315–2319.

Guo, G., Yang, J., Nichols, J., et al. (2009). Klf4 reverts developmentally programmed restriction of ground state pluripotency. Development *136*, 1063–1069.

Hanna, J., Markoulaki, S., Mitalipova, M., et al. (2009). Metastable pluripotent states in NOD-mouse-derived ESCs. Cell Stem Cell *4*, 513–524.

Haub, O., and Goldfarb, M. (1991). Expression of the fibroblast growth factor-5 gene in the mouse embryo. Development *112*, 397–406.

Hayashi, K., Lopes, S.M., Tang, F., et al. (2008). Dynamic equilibrium and heterogeneity of mouse pluripotent stem cells with distinct functional and epigenetic states. Cell Stem Cell *3*, 391–401.

He, W., Miao, F.J., Lin, D.C., et al. (2004). Citric acid cycle intermediates as ligands for orphan G-protein-coupled receptors. Nature *429*, 188–193.

Kalmar, T., Lim, C., Hayward, P., et al. (2009). Regulated fluctuations in Nanog expression mediate cell fate decisions in embryonic stem cells. PLoS Biol. *7*, e1000149.

Makarenkov, V., Kevorkov, D., Zentilli, P., et al. (2006). HTS-corrector: software for the statistical analysis and correction of experimental high-throughput screening data. Bioinformatics *22*, 1408–1409.

Maltsev, V.A., Rohwedel, J., Hescheler, J., et al. (1993). Embryonic stem cells differentiate *in vitro* into cardiomyocytes representing sinusnodal, atrial and ventricular cell types. Mech. Dev. *44*, 41–50.

Martin, G.R. (1981). Isolation of a pluripotent cell line from early mouse embryos cultured in medium conditioned by teratocarcinoma stem cells. Proc. Natl. Acad. Sci. USA *78*, 7634–7638.

Masui, S., Nakatake, Y., Toyooka, Y., et al. (2007). Pluripotency governed by Sox2 via regulation of Oct3/4 expression in mouse embryonic stem cells. Nat. Cell Biol. *9*, 625–635.

McEwan, M., Lins, R.J., Munro, S.K., et al. (2009). Cytokine regulation during the formation of the fetal-maternal interface: focus on cell-cell adhesion and remodelling of the extra-cellular matrix. Cytokine Growth Factor Rev. *20*, 241–249.

Mitsui, K., Tokuzawa, Y., Itoh, H., et al. (2003). The homeoprotein Nanog is required for maintenance of pluripotency in mouse epiblast and ES cells. Cell *113*, 631–642.

Nakamura, K., Salomonis, N., Tomoda, K., et al. (2009). G_i-coupled GPCR signaling controls the formation and organization of human pluripotent colonies. PLoS One *4*, e7780.

Nash, R., Neves, L., Faast, R., et al. (2007). The lectin Dolichos biflorus agglutinin recognizes glycan epitopes on the surface of murine embryonic stem cells: a new tool for characterizing pluripotent cells and early differentiation. Stem Cells *25*, 974–982.

Niwa, H. (2007). How is pluripotency determined and maintained? Development *134*, 635–646.

Paglialunga, F., Fico, A., Iaccarino, I., et al. (2004). G6PD is indispensable for erythropoiesis after the embryonic-adult hemoglobin switch. Blood *104*, 3148–3152.

Pelton, T.A., Sharma, S., Schulz, T.C., et al. (2002). Transient pluripotent cell populations during primitive ectoderm formation: correlation of *in vivo* and *in vitro* pluripotent cell development. J. Cell Sci. *115*, 329–339.

Rathjen, J., Lake, J.A., Bettess, M.D., et al. (1999). Formation of a primitive ectoderm like cell population, EPL cells, from ES cells in response to biologically derived factors. J. Cell Sci. *112* (Pt 5), 601–612.

Rogers, M.B., Hosler, B.A., and Gudas, L.J. (1991). Specific expression of a retinoic acid-regulated, zinc-finger gene, Rex-1, in preimplantation embryos, trophoblast and spermatocytes. Development *113*, 815–824.

Semon, B.A., and Phang, J.M. (1991). Accumulation of pyrroline 5-carboxylic acid in conditioned medium of cultured fibroblast: stimulatory effects of serum, insulin, and IGF-1. Cell. Dev. Biol. *27A*, 665–669.

Shi, Y. (2007). Histone lysine demethylases: emerging roles in development, physiology and disease. Nat. Rev. Genet. *8*, 829–833.

Tesar, P.J., Chenoweth, J.G., Brook, F.A., et al. (2007). New cell lines from mouse epiblast share defining features with human embryonic stem cells. Nature *448*, 196–199.

Toyooka, Y., Shimosato, D., Murakami, K., et al. (2008). Identification and characterization of subpopulations in undifferentiated ES cell culture. Development *135*, 909–918.

Washington, J.M., Rathjen, J., Felquer, F., et al. (2010). L-proline induces differentiation of ES cells: a novel role for an amino acid in the regulation of pluripotent cells in culture. Am. J. Physiol. Cell Physiol. *298*, C982–C992.

Ying, Q.L., Nichols, J., Chambers, I., et al. (2003). BMP induction of Id proteins suppresses differentiation and sustains embryonic stem cell self-renewal in collaboration with STAT3. Cell *115*, 281–292.